

CHAPTER 2

CONTEXT AND MOTIVATIONS

In this chapter, we introduce information to contextualize the measurements of YbPdBi presented in later chapters. We begin with an introduction to the half-Heusler family of structures, a versatile noncentrosymmetric cubic structure. Fermiology, the study of the Fermi surface, is then reviewed. This is followed by a brief discussion of the Kondo Effect and heavy fermion materials and a brief introduction to topological materials focusing on Weyl semimetals. Finally, we discuss the reasons for which YbPdBi is of interest.

A thorough discussion of these topics is not our goal. We focus on details that relate most directly to our experimental results. An effort has been made to suggest resources for a more thorough discussion of advanced topics, and one may find further discussions by examining the various cited sources.

2.1 The Half-Heusler Structure

The Heusler family of structures can be thought of as four interpenetrating face-centred cubic (FCC) sublattices. The full Heusler and half-Heusler unit cells are shown in Fig. 2.1a and Fig. 2.1b, respectively. Each consecutive FCC sublattice is offset by repeated lattice translations of $[\frac{1}{4}, \frac{1}{4}, \frac{1}{4}]$. A full-Heusler typically has a compound name of the form XYZ_2 , where X and Y are transition metals and Z is a main group element or metalloid. A half-Heusler will similarly be named XYZ , with an ordered vacancy at the $[\frac{3}{4}, \frac{3}{4}, \frac{3}{4}]$ site. The half-Heusler structure belongs to space group $\bar{F}43m$, is noncentrosymmetric, and so lacks inversion symmetry.

Despite the simple geometry of their unit cell, Heusler compounds have a long history of

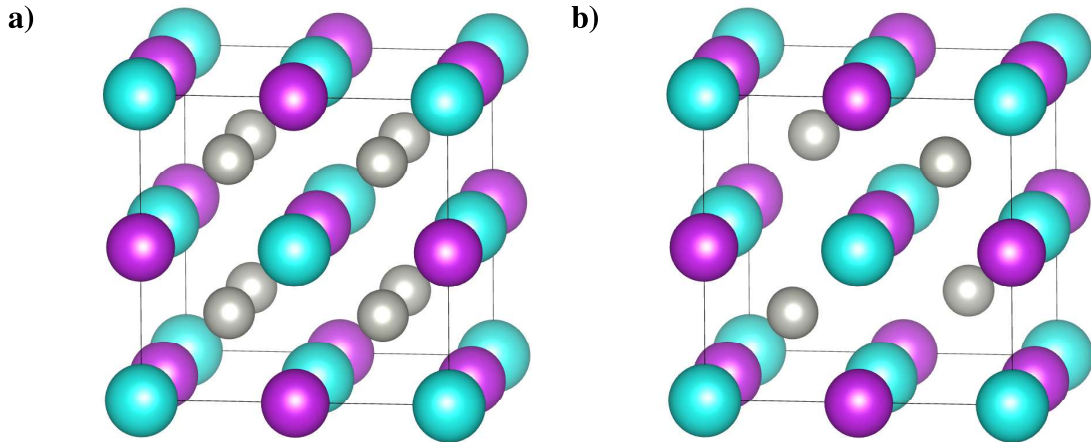


Figure 2.1 – (a) Full Heusler having naming scheme XYZ_2 . (b) Half-Heusler structure having the naming scheme XYZ . Constituents X and Y, shown in blue and purple, respectively, are typically transition metal elements. These are accompanied by a main group or metalloid element Z, shown in grey.

exhibiting interesting phenomena [5, 6], including ferromagnetic half-metallicity, high spin polarization, good thermoelectric performance, and non-trivial topology. It is predicted that the Heusler family can host tunable topology [7, 8]. Such tunability would make the Heusler family of compounds a source of multifunctional platforms for studying the interplay of topology and the aforementioned phenomena.

2.2 Fermiology and AMRO

2.2.1 The Fermi Surface

Fermiology is the study of a material’s Fermi surface (FS) and its effect on the properties of said material. The FS is defined as the isoenergetic surface in momentum space (k -space) which separates the occupied states from the unoccupied states at zero temperature. To construct such an isoenergetic surface, consider a simple cubic lattice with lattice constant a , with electrons restricted to nearest-neighbours hopping, and where each atom contributes only one valence electron to the conduction electrons. Ignoring spin, each electron will have a unique crystal momentum \vec{k} by which we may label it.

The tight-binding dispersion for this cubic lattice takes the form [9] :

$$E(k_x, k_y, k_z) = -\alpha - 2\gamma(\cos k_x a + \cos k_y a + \cos k_z a) \quad (2.1)$$

where a is the lattice constant, γ is the overlap integral (the energy associated with hopping from one lattice site to an adjacent lattice site), and α is the energy of the atomic orbital at each lattice site. Using this dispersion, we can construct an isoenergetic surface in k -space by selecting the set of momentum states having the desired energy. Shown in Fig. 2.2 in both the reduced and periodic zone schemes is a surface created with Eqn. 2.1 by the momentum states for which $E = -\alpha$. If it is also the case that $E = E_F$, then the surface shown in Fig. 2.2 is the Fermi surface of the cubic lattice.

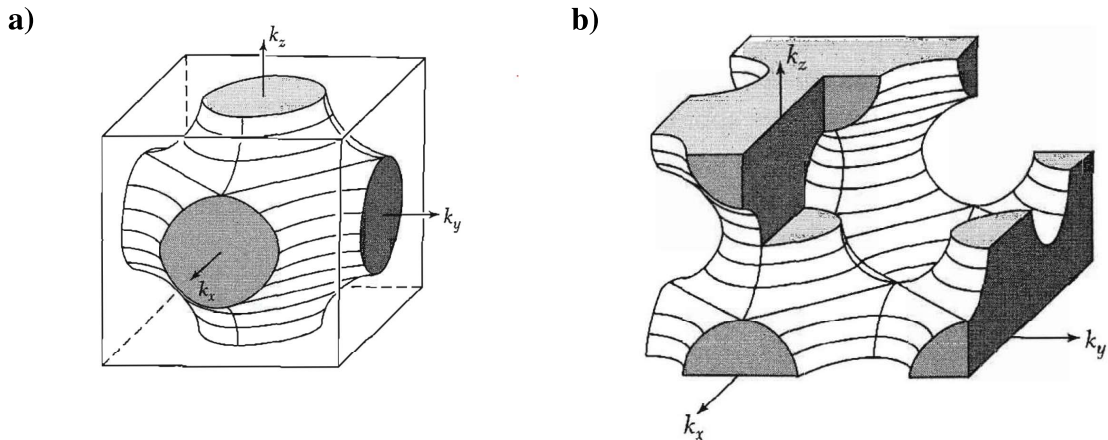


Figure 2.2 – An isoenergetic surface for free electrons in the first Brillouin Zone of a cubic lattice, given by Eqn. 2.1. (a) Shown in the reduced scheme is an isoenergetic surface made of the states for which $E = -\alpha$. (b) The same surface is shown in the periodic scheme. From *Introduction to Solid State Physics* (8th Edition, p. 231) by C. Kittel, 2004, Hoboken, NJ: John Wiley and Sons, Inc. Copyright 2005 by John Wiley and Sons, Inc [10]. Reprinted with permission.

If we slightly increase the system's temperature from absolute zero, states within $\sim k_B T$ in energy above and below E_F begin to be populated and depopulated, respectively. These electrons are those that participate in electron transport. Since the FS is representative of the electronic states available to these electrons, the structure of the FS plays

a crucial role in determining the electrical conductivity of a material. For example, the way in which the behaviour of insulators, metals, and semiconductors can be explained by how their bandstructures do or do not intersect E_F .

Should the system be placed in a magnetic field H (say, down the z -axis), the electrons will move along isoenergetic paths in a plane orthogonal to H (the xy -plane) due to the Lorentz force. Since the FS is a surface of constant energy, the conduction electrons will take paths around the FS. These paths along the Fermi surface may be classified as either closed or open orbits.

Closed orbits confine the electron to a path that remains within the boundaries of the First Brillouin Zone (FBZ). Closed orbits may be further classified into holelike orbits and electronlike orbits. These are determined by whether the closed orbit encloses unoccupied or occupied states, respectively, and changes the direction that \vec{k} rotates relative to H as the electron traces the path. Since we are only considering paths along the FS, a closed orbit will not partially enclose occupied states.

Open orbits take the electron along a path from one boundary of the FBZ to another boundary. They play an important role in determining the magnetoresistance of a material [10]. Electrons taking paths along open orbits will not be deflected by H , as they are confined to move in one direction in k -space by the topology of the path.

Finally, the effective mass of the electrons in a particular band is inversely proportional to the curvature of the band dispersion [11] :

$$(m^*)^{-1} = \frac{1}{\hbar} \frac{d^2 E(k)}{dk^2} \quad (2.2)$$

where \hbar is the reduced Planck's constant. Let us consider an example to illustrate the relationship between the FS and m^* of conduction electrons. Recall the dispersion for the cubic lattice given in Eqn. 2.1 and consider the line in k -space for which $k_z = k_y = \pi/a$.

For this line, m^* can be obtained using Eqn. 2.2 :

$$E(k_x) = -\alpha - 2\gamma \cos(k_x a) \quad (2.3)$$

$$\implies (m^*)^{-1} = \frac{2\gamma}{\hbar} k_x^2 a^2 \cos(k_x a) \quad (2.4)$$

where we see that m^* of a state is dependent on its momentum, and can be parametrized by this system's γ . Should this dispersion describe the conduction band of the system, m^* of the conduction electrons will be large when γ is small. In this case, γ also parametrizes the amplitudes of the cosine functions and so affects the curvature of the band. This example makes it clear how flat bands will result in large effective masses due to their small curvature. The FS plays an important role in heavy fermion materials, which we will discuss further in Sec. 2.3.2.

2.2.2 Probing the Fermi Surface

A number of experimental and theoretical methods are available to probe the FS of a material. Unlike with the fairly simple cubic lattice of the previous section, calculating the bandstructure of a real material with high precision can be complicated. This is foremost because we are interested in materials that have strong electron-electron interaction terms, for which we lack a complete microscopic description of their physics.

One particularly useful technique for studying the bandstructure is *ab initio* density functional theory (DFT) calculations [12]. In essence, DFT uses functionals of the electron density and a model Hamiltonian of the material to approximate a material's bandstructure. To improve or test the model used by a given DFT calculation, the results are often compared against angle-resolved photoemission spectroscopy (ARPES) measurements.

ARPES provides the most direct probe of a FS and of the bandstructure in general. These measurements are direct mappings of a material's bandstructure via the photoelectric effect [13]. ARPES typically requires the experimenter to apply for beamtime

at synchrotron facilities where photons are made in the UV range. There has been some success in addressing this issue through the development of laser-based tabletop ARPES systems [14–16] for which the photon energy is less than for synchrotrons. Though this improves sensitivity to bulk states, the reduced photon energy has trouble measuring the surface states, which presents issues for experiments involving topologically non-trivial matter.

The FS has historically been probed via quantum oscillation experiments. Such experiments leverage the quantized nature of electron orbits in a magnetic field (i.e. Landau levels) [11]. Oscillations of a sample’s magnetization as a function of the inverse magnetic field ($1/H$) comprise the de Haas-van Alphen effect (dHvA). These magnetization oscillations will oscillate about a background curve that must be approximated and subtracted from the data. Similar oscillations in the resistivity as a function of $1/H$ comprise the Shubnikov-de Haas effect (SdH).

One can infer the extremal cross-sectional area of the FS from the period of these oscillations in $1/H$. This cross-sectional area will be in a plane orthogonal to H , and the FS can be roughly mapped by rotating H relative to the sample. Unfortunately, quantum oscillation methods can require large magnetic fields ($\mu_0 H > 10$ T) and/or high-precision measurements of the oscillating quantity.

Considering the importance of the FS in determining interesting properties of a material, it would be useful to have a “quick-and-dirty” means of probing the FS. Such a method would augment DFT in identifying materials suitable for ARPES. It would also be sensitive to changes in the FS due to H , such as in the case of a field-induced Lifshitz transition. Angle-resolved magnetoresistance oscillations (AMRO) are one potential tool that addresses these issues.

2.2.3 Angle-Resolved Magnetoresistance Oscillations

Angle-resolved magnetoresistance (AMR) describes the change in the resistivity ρ of a sample under a constant magnetic field H as a function of the sample's orientation θ with respect to H . Periodic oscillations in ρ that occur during this rotation are called angle-resolved magnetoresistance oscillations (AMRO). AMRO experiments have notably been used to demonstrate that the high-temperature superconductors (HTSC's) possess a FS [17], when it was still unclear whether they indeed possessed one. HTSC's are poor metals when not in a superconducting state, and the fields required for dHvA experiments were of order $\mu_0 H = 100$ T.

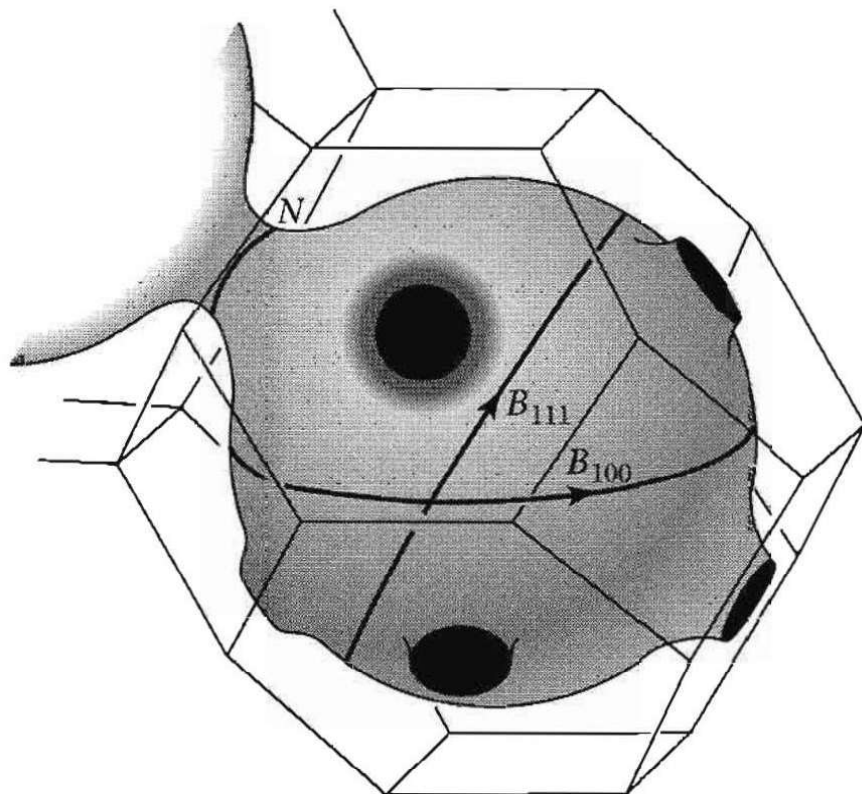


Figure 2.3 – Fermi surface of copper (Cu) within the First Brillouin Zone. From *Introduction to Solid State Physics* (8th Edition, p. 250) by C. Kittel, 2004, Hoboken, NJ: John Wiley and Sons, Inc. Copyright 2005 by John Wiley and Sons, Inc [10]. Reprinted with permission.

AMRO has the advantage of immediately measuring the symmetry of the FS. For an idealized spherical FS, we can infer that rotating the sample will not produce observable changes in the measured ρ . The FS has full rotational symmetry, and so the orbits available to the electrons are equivalent for any orientation θ . However, a real FS for a real material will have lower symmetry than a perfect sphere.

As an example, consider the FS of copper (Cu), shown in Fig. 2.3, which is symmetrical under 90° rotations. We apply a magnetic field H vertically. A current of electrons will move orthogonal to H along the closed orbit B_{100} about the equator of the FS. We next rotate the sample by some angle $\theta < 90^\circ$. The paths of the electrons also rotate to remain confined to planes orthogonal to H . The electrons previously taking path B_{100} now move along the closed orbit B_{111} , again about the equator of the FS.

Though the orbits B_{100} and B_{111} happen to be similar, the observable magnetotransport properties of the system will have changed. All paths about the FS are involved in magnetotransport and not all paths will have been rotated into an orbit similar to their initial orbit. We can see this by the addition of closed orbit N about the neck at the boundary of the FBZ. Further, we can clearly see that between B_{100} and B_{111} , there lays a set of open paths about the FS. Therefore, as we rotate the system through this range of θ , the magnetotransport properties will be changing because the electrons confined to the rotating path will have moved along open orbits during part of the rotation.

We may conclude that for a non-isotropic FS in constant magnetic field H , the paths available to the conduction electrons will possess a dependence on the sample's orientation θ relative to H . This will be observable in the behaviour of ρ with a θ dependence that reflects the symmetry of the FS, which is also the symmetry of the lattice. More explicitly, it has been shown that the components of the conductivity tensor for band electron states in a constant, uniform magnetic field can be calculated using the Chambers formula [11, 18–20]. This formula is a solution to the Boltzmann transport equation and relates the conductivity to the FS.

2.3 Heavy Fermion Materials

We begin this section by introducing the Kondo effect, wherein a magnetic impurity is embedded in a conductive lattice. This is followed by the topic of heavy fermion materials, which can be thought of as a lattice of Kondo ions. These possess many magnetic impurities, and the conduction electrons have greatly enhanced effective masses. Finally, we briefly present the phenomenological two-fluid model for heavy fermion systems. It has found some success in describing the observed phenomena of heavy fermion materials, which do not yet have a thorough microscopic model.

An excellent introduction to these topics has been written by the eponymous Jun Kondo [21]. A thorough discussion of the models and work related to the Kondo problem is given in the textbook “The Kondo Problem to Heavy Fermions” by Alexander Hewson [22]. A reasonably up-to-date discussion of the microscopic theory, including the two-fluid model, is presented by Gilbert Lonzarich, David Pines, and Yi-Feng Yang [23].

2.3.1 The Kondo Effect

The Kondo effect is fundamental to understanding heavy fermion systems [21]. It can be understood as the change in the temperature-dependence of the resistivity ($\rho(T)$) of a metallic lattice by the introduction of a magnetic impurity, which differs significantly from that for non-magnetic impurities. In this context, we describe a magnetic impurity as a spatially localized magnetic moment within the metallic lattice [11]. This is realized in the form of a transition metal or lanthanide metal element that possesses at least one unpaired electron in its d - or f -shell, respectively.

We can see the effect of impurities on $\rho(T)$ in Fig. 2.4. The behaviour of $\rho(T)$ for a metallic lattice with no impurities is shown in Fig. 2.4a, where it monotonically ap-

proaches zero as T goes to zero. In this case, scattering off phonons is the dominant source of resistance, and the phonons are frozen out as the material cools. Fig. 2.4b shows the effect of a non-magnetic impurity, which results in a non-zero residual resistivity and a curve that still decreases monotonically as the phonons are frozen out. Finally, Fig. 2.4c shows the behaviour of $\rho(T)$ when the impurity is magnetic. Here, a minimum resistivity is reached at a low temperature (of order $T \sim 10$ K or so), below which the resistivity begins to increase. The causal relationship between the presence of the magnetic impurity and this minimum encapsulates the Kondo Problem.

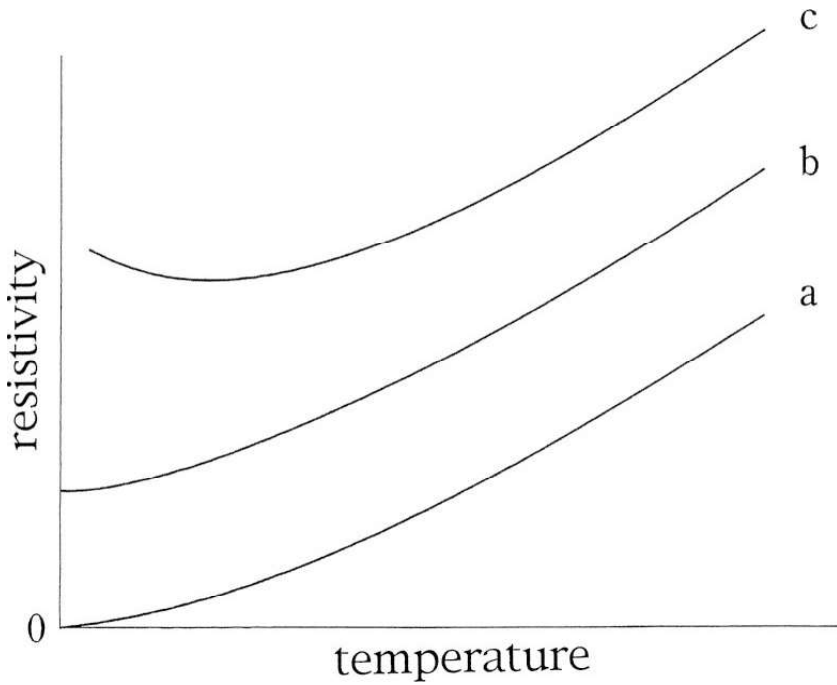


Figure 2.4 – Resistivities $\rho(T)$ for a metal with: (a) No impurities; (b) A non-magnetic impurity; (c) A magnetic impurity. From "Resistance minimum and heavy fermions," by J. Kondo, 2006, *Proceedings of the Japan Academy, Series B: Physical and Biological Sciences*, 82, 328-338. CC-BY [21].

Real-world examples of this minimum are shown in Fig. 2.5, where magnetic iron (Fe) atoms have been dissolved into a copper (Cu) lattice at concentrations of 0.2 %, 0.1 %, and 0.05 %. These Fe atoms act as magnetic impurities within the metallic lattice. Increasing the concentration of the magnetic Fe impurities increases the difference be-

tween residual resistivity and the minimum value. In this figure, R_0 is the resistivity value at $T = 273.15$ K.

In 1964, Jun Kondo showed that this resistance minimum can be derived from the s-d interaction model [21, 22, 25] :

$$H = H_{KE} + H_{sd} \quad (2.5)$$

$$H_{KE} = \sum_{\mathbf{k}, \sigma} \epsilon_{\mathbf{k}} c_{\mathbf{k}, \sigma}^{\dagger} c_{\mathbf{k}, \sigma} \quad (2.6)$$

$$\begin{aligned} H_{sd} = & \sum_{\mathbf{k}, \mathbf{k}'} J_{\mathbf{k}, \mathbf{k}'} \left(S^+ c_{\mathbf{k}, \downarrow}^{\dagger} c_{\mathbf{k}', \uparrow} + S^- c_{\mathbf{k}, \uparrow}^{\dagger} c_{\mathbf{k}', \downarrow} \right. \\ & \left. + S_z \left(c_{\mathbf{k}, \uparrow}^{\dagger} c_{\mathbf{k}', \uparrow} - c_{\mathbf{k}, \downarrow}^{\dagger} c_{\mathbf{k}', \downarrow} \right) \right) \end{aligned} \quad (2.7)$$

where H_{KE} is the kinetic energy of the conduction electrons and H_{sd} is the exchange interaction term. The interaction is antiferromagnetic, so $J_{\mathbf{k}, \mathbf{k}'} < 0$. Both S_z and $S^{\pm} = S_z \pm iS_y$ are spin operators for an impurity state of spin S . The operator $c_{\mathbf{k}\sigma}^{\dagger}$ is a creation operator for a conduction electron of momentum \mathbf{k} with spin σ and energy $\epsilon_{\mathbf{k}}$. The corresponding annihilation operator is $c_{\mathbf{k}\sigma}$. Note that we are succumbing to a desire to avoid over-cluttering the notation, and so are omitting “hats” from the operator notation. The notionally precise form of these operators would appear as $\hat{O}_{\mathbf{k}, \sigma}$.

The H_{sd} term describes a Heisenberg exchange interaction between the conduction electrons and a localized moment/impurity with spin S . The first two terms of H_{sd} impose that the interaction will flip the spin of both the impurity and the conduction electron (for an impurity with $S > 1/2$, the spin will instead be raised/lowered). The third term in H_{sd} imposes an energy cost for spin-preserving interactions between spins of opposite orientations. It was shown by Coqblin and Schrieffer [26] that the s-d model is related to the Anderson model, which has been used in attempts to describe heavy fermion materials. We briefly discuss the Anderson model in Sec. 2.3.2.

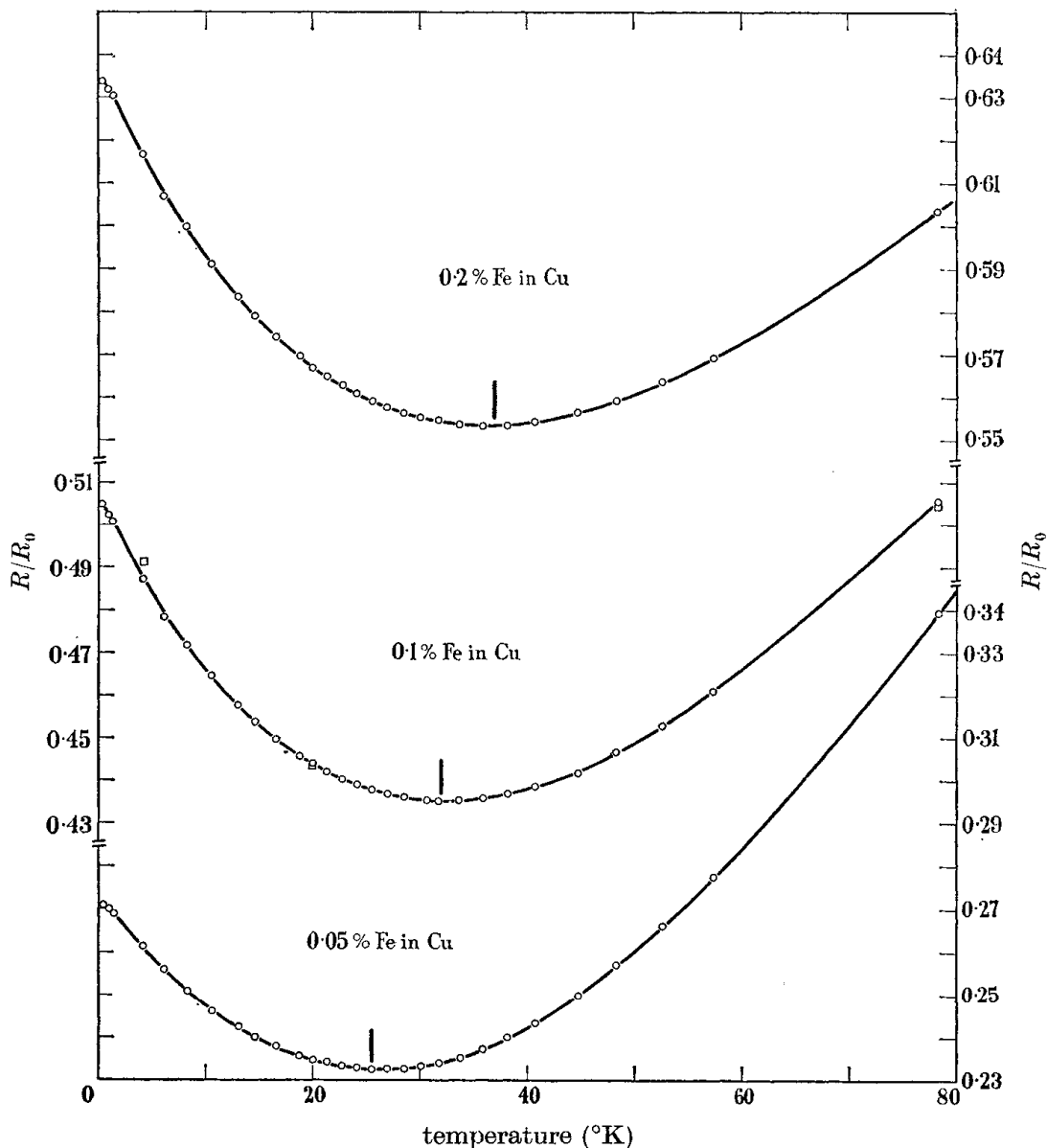


Figure 2.5 – Examples of resistivity (R/R_0) minima caused by the dissolution of magnetic iron (Fe) impurities into a copper (Cu) lattice. In this figure, R_0 is the resistivity measured at $T = 273.15$ K. The units on the bottom of the right axis correspond to the 0.05 % concentration, the units on the left vertical axis correspond to the 0.1 % concentration, and the units on the top right axis correspond to the 0.2 % concentration. Public domain figure reprinted from [24].

Before Kondo, the issue of scattering off magnetic impurities had only been treated up to leading order in perturbation theory [11]. The calculated resistivities didn't differ significantly from the results for non-magnetic impurities. Spin-flip scattering events were also neglected. Kondo included these and was able to show that the resistivity contribution from the magnetic impurities is of the form of $-c \log T$, where c is the concentration of magnetic impurities. This is the case for any magnetic impurity off which conduction electrons scatter, so long as the exchange interaction J is AFM. At high temperatures, the logarithmic term is negligible in comparison to the phonon scattering contribution. As the temperature T is lowered, the phonons are frozen out, and this impurity term becomes dominant before eventually diverging at absolute zero. The temperature-dependent balance between the phonon and impurity contributions results in the resistance minimum. The antiferromagnetic scattering of conduction electrons by magnetic impurities, and the resulting in a resistivity minimum, have since been dubbed Kondo scattering and the Kondo Effect.

So far, we have only considered $\rho(T)$ curves for dilute magnetic alloys, where the concentration of magnetic impurities is small (i.e. less than $\sim 1\%$ of the total atoms). At such low concentrations, interactions between the magnetic impurities can be neglected. At higher concentrations, the interactions between magnetic impurities have a significant impact, and a Kondo Lattice is formed. This will typically result in the creation of a heavy fermion compound.

2.3.2 Heavy Fermion Materials

When a lattice of localized magnetic impurities is embedded within a metallic lattice, with a concentration above a few percent of the total lattice ions, a Kondo lattice is formed. The individual magnetic moments begin to act coherently, which affects the Kondo scattering such that a heavy fermion material (HFM) is formed [27]. These materials exhibit a number of interesting physical properties, namely a greatly enhanced effective mass for the conduction electrons.

A key observable of HFM's is a sharp decrease in the resistivity as the temperature is lowered below a characteristic temperature, called the coherence temperature T^* . Lowering the temperature while above T^* , the resistivity increases due to Kondo scattering. Below T^* , the magnetic moments begin to act coherently, and the resistivity drops quickly. We define T^* as the temperature at which the resistivity maximum occurs. This behaviour is due to the formation of heavy fermion quasiparticles (HFQPs) by the conduction electrons hybridizing with the magnetic moments into a Kondo coherent state.

Shown in Fig. 2.6 is what occurs to the resistivity of $\text{Ce}_x\text{La}_{1-x}\text{Cu}_6$ when the concentration of magnetic impurities is increased. As the doping parameter x is increased, non-magnetic lanthanum (La) is replaced by magnetic cerium (Ce). At $x = 0.094$ and $x = 0.5$, we can clearly see the resistivity minimum of the Kondo effect. As x continues to be increased, a maximum resistivity begins to occur in the curve, below which there is a sharp decrease and a return to metallic-like behaviour.

For a HFM, the greatly enhanced effective mass of the conduction electrons is inferred primarily by observation of a Sommerfeld coefficient γ that is orders of magnitude larger than that of copper (Cu). We measure γ using low-temperature measurements of the specific heat (C_p) [11] :

$$C_p = \gamma T + \beta T^3 \quad (2.9)$$

where γ characterizes the conduction electron contribution and β characterizes the phonon contribution. An excellent example of this is the specific heat for YbPtBi (isostructural to YbPdBi) with a value of $\gamma \sim 8 \text{ J/mol-K}$ for YbPtBi, which suggests an effective mass 8000 times larger than Cu [3].

To garner an understanding of heavy fermion materials, one can build upon the physics of the Kondo effect. It is curious that HFM behaviour occurs as the concentration of magnetic impurities is increased. It was the initial addition of magnetic impurities and

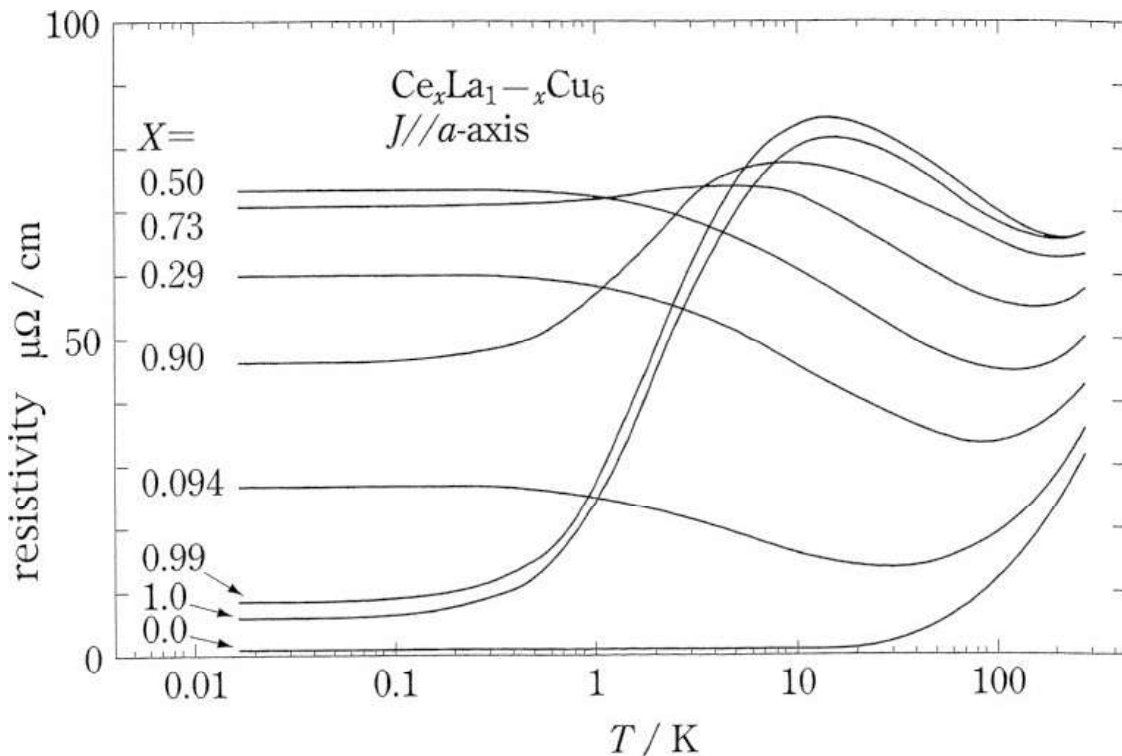


Figure 2.6 – Resistivity plot of $\text{Ce}_x\text{La}_{1-x}\text{Cu}_6$. For increasing values of x , magnetic cesium (Ce) increasingly replaces non-magnetic lanthanum (La) in the lattice. From "Resistance minimum and heavy fermions," by J. Kondo, 2006, *Proceedings of the Japan Academy, Series B: Physical and Biological Sciences*, 82, 328-338. CC-BY [21].

the Kondo Effect that caused the resistivity minimum. Why, then, should the further addition of magnetic impurities cause such a drastic change?

The answer rests on the idea that we can no longer treat the magnetic impurities as isolated from one another. The interactions between the impurities are now a significant factor in determining the physical properties of the material. One model that has been used in attempts at finding microscopic descriptions of heavy fermion materials is the

periodic Anderson model, which takes the form [22] :

$$H = H_{KE}^c + H^f + H_{Coul.} + H_{Hyb}. \quad (2.10)$$

$$H_{KE}^c = \sum_{\mathbf{k}, \sigma} \varepsilon_{\mathbf{k}} c_{\mathbf{k}\sigma}^\dagger c_{\mathbf{k}\sigma} \quad (2.11)$$

$$H^f = \sum_{i, \sigma} \varepsilon_f c_{f,i,\sigma}^\dagger c_{f,i,\sigma} \quad (2.12)$$

$$H_{Coul.} = U \sum_i n_{f,i,\uparrow}^\dagger n_{i,\downarrow} = U \sum_i c_{f,i,\uparrow}^\dagger c_{f,i,\uparrow} c_{i,\downarrow}^\dagger c_{i,\downarrow} \quad (2.13)$$

$$H_{Hyb.} = \sum_{i, \mathbf{k}, \sigma} \left(V_{\mathbf{k}} e^{i \mathbf{k} \cdot \mathbf{R}_i} c_{f,i,\sigma}^\dagger c_{\mathbf{k},\sigma} + V_{\mathbf{k}}^* e^{-i \mathbf{k} \cdot \mathbf{R}_i} c_{\mathbf{k},\sigma}^\dagger c_{f,i,\sigma} \right) \quad (2.14)$$

where H_{KE}^c is the kinetic energy of delocalized conduction electrons with momentum \mathbf{k} , spin σ , and energy $\varepsilon_{\mathbf{k}}$. H^f is the energy of the localized f -electrons at sites i with spin σ , each one having energy ε_f . $H_{Coul.}$ is the Coulomb repulsion of strength U between electrons at each site i , which has an f -electron. $H_{Hyb.}$ describes the hybridization between the localized f -electrons at sites \mathbf{R}_i and delocalized conduction electrons. A reminder that an electron in a localized state will have a well-defined position. Conversely, an electron in a delocalized state will not have a well-defined position.

A full description of heavy fermion materials at the microscopic level remains to be found. It is complicated by the fact that some heavy fermion materials exhibit unconventional superconductivity, quantum criticality, non-Fermi liquid behaviour, and non-trivial topology [22, 28]. This motivates both the theoretical and experimental exploration of HFM's.

Here, we would like to mention the recent evidence for Weyl semimetal (WSM) behaviour in the canonical heavy fermion YbPtBi [4]. This suggests that HFM's can also host non-trivial topology. A WSM in a HFM results in a material called a Weyl-Kondo semimetal (WKSM). Since Weyl fermions are massless quasiparticles with spin-1/2, their potential coexistence with HFQP is an interesting phenomenon.

Evidence for or against chiral HFQPs should be observable in the magnetotransport. If the HFQP have chirality, then they will experience a chiral anomaly in a magnetic field and so will undergo chiral transport. Derivation of such observables is beyond the scope of this work, and so we must leave these questions unanswered, but a recent paper [29] deriving the specific heat for a WKSM using the periodic Anderson model should be an excellent starting place.

2.3.3 Two-Fluid Model

One model that has found some success in describing how the Kondo coherent state forms is the two-fluid model (2FM) [28, 30]. Analogous to the 2FM for superfluid helium, this phenomenological model describes a fluid of itinerant HFQPs existing alongside a fluid of localized magnetic moments. The itinerant HFQPs of the first fluid are heavy due to the hybridization between conduction electrons and some localized moments. The remaining local moments of the second fluid have not yet hybridized with conduction electrons. The total amount of fluid is a conserved quantity, and the relative amount of each constituent fluid is parametrized by the temperature T , a key parameter of the 2FM.

The most important aspect of this model is that, as the temperature is lowered, the amount of itinerant HFQP fluid grows while the fluid of local moments shrinks. Experiments have shown the hybridization process exhibits a universal temperature dependence parametrized by the fraction of HQFP fluid to total fluid [30] :

$$f(T) = f_0 \left(1 - \frac{T}{T^*}\right)^{3/2} \quad (2.15)$$

where hybridization effectiveness f_0 determines how quickly the electrons hybridize with the local moments as the temperature is dropped. Both f_0 and T^* have been shown to vary with tuning parameters such as magnetic field or pressure.

Such two-fluid behaviour is supported by experimental evidence in a number of heavy fermion materials [23, 28]. This universal scaling has been observed in the Knight shift anomaly and the Nernst coefficient in a number of heavy fermion compounds, and in the Hall coefficient for Ce-based compounds [28].

2.4 Topological Materials

In this section, we give a brief overview of topology in the context of condensed matter, with a focus on Weyl semimetals (WSM's). This will lay the foundation for introducing the experimental signatures of a WSM. The theory behind topological matter is rich and expansive, but it can also be rather formidable and complex. We will, therefore, strive to limit ourselves to the details most pertinent to our experimental results.

For those seeking a more detailed discussion of condensed matter topology, we suggest the following resources. Regarding topological insulators (TI's), we suggest reviews by Hasan and Kane [31] and R. Shankar [32]. For WSM's we suggest Yan and Felser [33] or Jia *et al.* [34] for a cursory introduction, and Armitage, Mele, and Vishwanath [35] for a more thorough review. If one is seeking a pedagogical approach for graduate students, Girvin and Yang [36] have written a textbook which devotes multiple chapters to all the aforementioned topics and condensed matter theory in general.

Nonetheless, we would be remiss if we did not introduce at least some pertinent terminology:

Non-Triviality: One may classify insulators by the topology of their bandstructure [37]. A non-trivial insulator has non-trivial topology, which implies topologically protected invariants for the system exist. A trivial insulator, such as a vacuum, has trivial topology.

Band Inversion: Consider Fig. 2.7a, where two quadratic bands are intersecting. This

band inversion can be induced by turning on spin-orbit coupling (SOC), causing some states of the conduction band to join the valence band and vice versa. This reversal of the expected ordering of the conduction and valence bands is one way to think of the onset of non-trivial topology.

Bulk-Boundary Correspondence: One of the remarkable properties of non-trivial matter is that there exist exotic states in the bandstructure of the material's surface. In the bulk of a TI, there is a gapped, insulating bandstructure. On the surface of a TI, there exists a gapless, conducting bandstructure. Essentially, these gapless surface states form because the vacuum is a trivial insulator, and a topological phase transition must occur at the boundary separating the non-trivial insulator from the topological trivial vacuum.

Gapped/Gapless Bandstructure: Recall that an insulator can be defined as a material which has a gap in its density of states at E_F . If a band inversion is also present, the system is a TI with gapless surface states which have the bandstructure of a two-dimensional Dirac semimetal (DSM). A DSM can be thought of as the gapless midpoint in the band inversion. Non-trivial materials that are gapless in the bulk can also form, such as non-trivial semimetals. Three-dimensional DSM's and WSM's fall into this category and possess gapless surface states. For the bulk bandstructure of a WSM, shown in Fig. 2.7b, there exist pairs of points called Weyl nodes or Weyl points where the bandstructure is gapless. Weyl nodes always form in pairs of opposite chirality, which determines whether they act as sources or sinks of Berry curvature. The corresponding WSM surface states manifest as unclosed lines at the Fermi energy, which connect the projections of the Weyl points in the 2D bandstructure of the surface.

Topological Protection: The way in which topological invariants are “robust” to changes of the system Hamiltonian. If you change the Hamiltonian of a system for which there is a topological invariant, that invariant will only change if the system experiences a quantum phase transition which changes the topology of the system.

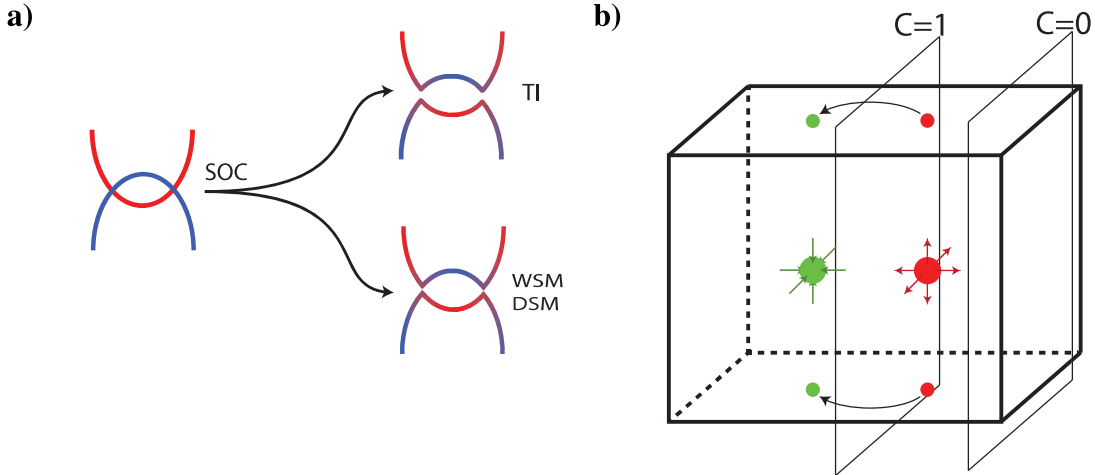


Figure 2.7 – (a) Band inversion leading to the non-trivial topology of a topological insulator (TI), a Weyl semimetal (WSM), or a Dirac semimetal (DSM). (b) Bulk states and surface states of a WSM. Weyl points act as sources (red) and sinks (green) of Berry curvature. Fermi arcs occur in the surface bandstructure at the Fermi energy and connect the projections of the Weyl points. In this example, a plane between the two Weyl points has a Chern number of $C = 1$, whereas all other planes have a $C = 0$ due to each plane's net Berry phase.

2.4.1 Weyl semimetals

Weyl fermions were initially introduced to describe massless relativistic particles in a vacuum, much like the Dirac equation was for massive particles. Though all particles of the Standard Model are Dirac fermions, Weyl fermions may be realized in condensed matter systems in the form of the WSM.

WSM's are materials for which the low-energy states near E_F disperse linearly in three dimensions. These low-energy states may be described by the 3D Weyl Hamiltonian [36] :

$$H = \pm v_F (\vec{\sigma} \cdot \vec{k}) \quad (2.16)$$

where v_F is the Fermi velocity (which defines the slope of the linear dispersion) and $\vec{\sigma} = (\sigma_x, \sigma_y, \sigma_z)$ are the Pauli matrices. A WSM is closely related to a DSM. In fact, Eqn. 2.16 is essentially just the Dirac Hamiltonian for a massless particle. A Weyl

fermion quasiparticle is half of a charged Dirac fermion with the addition of either a left- or right-handed chirality. Two Weyl fermions of opposite chirality may be combined to form one Dirac fermion.

For a WSM, the density of states (DoS) vanishes at a topologically protected node fixed to E_F , which is called a Weyl point or a Weyl node. Unlike a DSM, which can have a gap introduced to the DoS by including something like a mass term to the Hamiltonian, doing so for a WSM will move the node around in k -space. Such topological protection stems from the fact that in a WSM, each Weyl node acts as a source or sink of Berry flux (depending on the chirality of the node) [36]. The chiral nature of the nodes also enforces that the Weyl nodes will always occur in pairs.

Much like the surface states of TI's, the non-trivial topology of the WSM also results in gapless surface states that are topologically protected. These surface states form distinctive structures known as Fermi arcs, which connect projections of the Weyl nodes onto the surface. A candidate material is verified to be a WSM by the observation of Fermi arcs in the bandstructure of the surface. One may also observe the effects of the magnetic chiral anomaly in bulk transport measurements, but this is less conclusive.

2.4.2 Weyl semimetal Experimental Signatures

In non-orthogonal magnetic (B) and electric (E) fields, the particle number of Weyl fermions of a given chirality is not conserved. This results in the Adler-Bell-Jackiw anomaly, also known as the chiral anomaly [38–41]. The chiral anomaly is expected to result in a chiral conductivity of the form [42] :

$$\sigma_{CM}^{zz} \propto \frac{v_F^3 \tau_V}{T^2 + \frac{\mu^2}{\pi^2}} B^2 \quad (2.17)$$

where v_F is the Fermi velocity near the Weyl points, τ_V is the chirality-changing scattering time, T is the temperature, and $\mu = (\mu_R - \mu_L)/2$ is a function of the chemical

potentials of the right- and left-handed Weyl fermions. The resulting large negative longitudinal magnetoresistance (LMR) has been observed in a range of WSM's [37].

Though observing a large negative LMR with quadratic B dependence is a strong indicator of the chiral anomaly, it could originate from other causes that are not topological in nature [37]. One requires clear evidence of Weyl nodes in the bulk and Fermi arcs on the surface, which can be revealed by ARPES methods, as explained in Sec. 2.2. However, magnetotransport experiments are important for motivating and justifying these ARPES measurements.

Additional inferential evidence for WSM's may be obtained in the transverse resistivity ρ_{xy} . One can extract a contribution from a topological Hall effect and signs of the chiral anomaly in the planar angle-resolved magnetoresistance (PAMR) [4]. For Weyl-Kondo semimetals (WKS), low-temperature measurements of the specific heat ($T < 10$ K) can also show evidence for the existence of Weyl nodes [4, 29].

2.5 YbPdBi

YbPdBi is a member of the half-Heusler family, forming into space group $F\bar{4}3m$. It is noncentrosymmetric and thus lacks inversion symmetry, meaning YbPdBi can potentially host Weyl semimetal physics without needing a magnetic field. Bandstructure calculations have suggested the LnPdBi family (Ln=lanthanide element) may be capable of hosting tunable topology [7, 8]. Since including these lanthanides in a compound can also result in unique magnetism and unconventional superconductivity, it is possible that they can act as multifunctional platforms to study the interplay between topology and these phenomena. Further, the flux growth recipe for YbPdBi is simple and can be easily modified to include other rare earth elements (see Sec. 3.2). This allows one to dope the material to shift E_F and/or tune it away from heavy fermion behaviour.

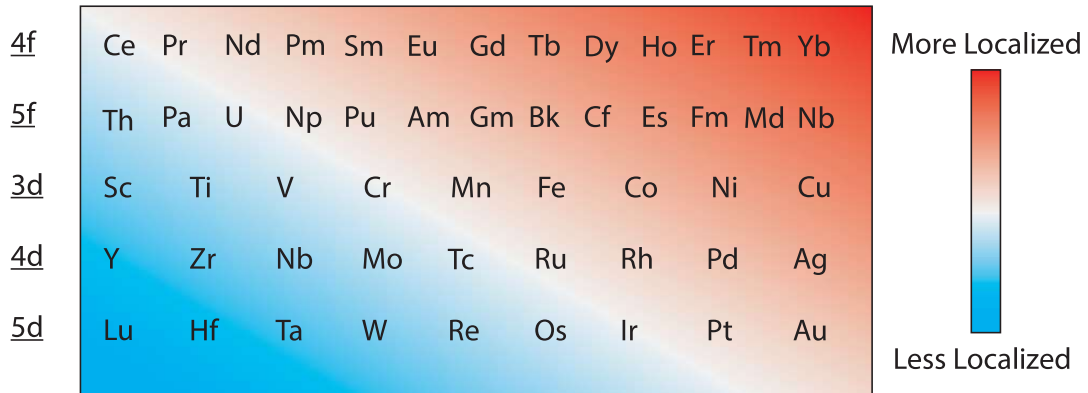


Figure 2.8 – A Kmetko-Smith diagram showing the general orbital localization trends for various transition metals, actinides, and rare earth elements.

YbPdBi is also isostructural to YbPtBi , the ‘heaviest’ HFM yet discovered [3]. Ytterbium (Yb) based heavy fermion materials are comparable to the more well-studied cerium (Ce) based heavy fermion compounds. Since the $4f$ -electrons of the Yb atoms are more localized than those in Ce. This localization affects the hybridization process that produces the HFQP, but the exact details of the relationship are still a topic of research. Both Yb^{3+} and Ce^{3+} possess a single unpaired electron in the $4f$ shell, but the free ion total angular momentum J is greater in Yb^{3+} ($J = 7/2$ versus $J = 5/2$). This leads to stronger spin-orbit coupling (SOC) in Yb-based compounds.

Finally, we believe YbPdBi is a possible Kondo-Weyl candidate, where a heavy fermion material also hosts WSM physics [29]. The aforementioned YbPtBi has shown evidence of being a WKSM in magnetotransport, ARPES, and specific heat measurements [4]. We believe the similarity between the compounds provides adequate motivation to check for signs of a chiral anomaly in YbPdBi . Should YbPdBi prove to host non-trivial topology, characterization may lead to insights regarding the interplay between heavy fermion physics and WSM’s.